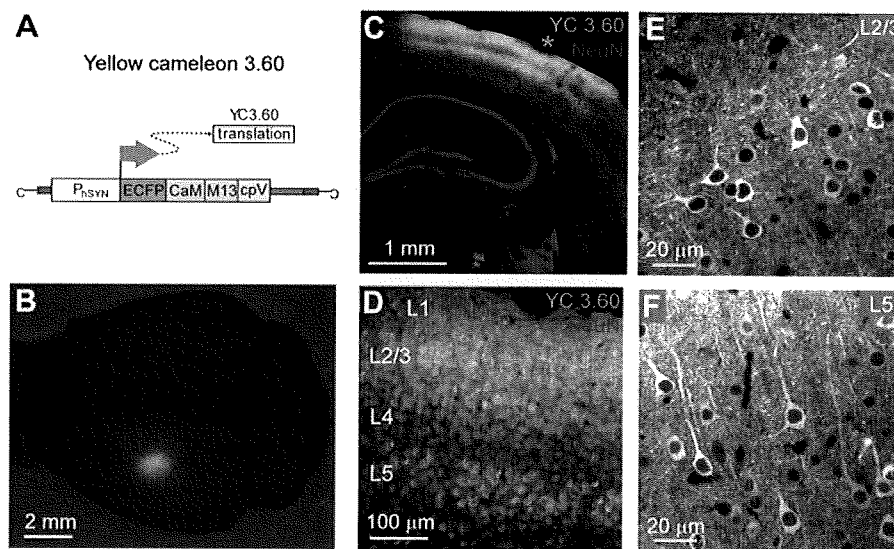


### 3. Results

#### 3.1. AAV-induced expression of the $\text{Ca}^{2+}$ sensor YC3.60 in mouse barrel cortex

Yellow cameleon 3.60 is a genetic  $\text{Ca}^{2+}$  sensor based on a CFP, a  $\text{Ca}^{2+}$ -sensitive linker, and a bright circularly permuted YFP (Nagai et al., 2004). Here, we characterized YC3.60 as a promising candidate protein for reporting neuronal activity in the mammalian cortex in vivo. We expressed YC3.60 in mouse barrel cortex under control of a human synapsin promoter using a recombinant adeno-associated virus (rAAV) vector (Figure 1A).



**Figure 1. AAV-delivered expression of YC3.60 in mouse neocortex**

(A) A recombinant adeno-associated virus with the human synapsin promoter ( $P_{hSYN}$ ) drives expression of YC3.60. (B) Dorsal view of a fixed mouse brain 4 weeks following stereotactic AAV-injection showing YC3.60 expression as a bright YFP fluorescence spot in barrel cortex in the left hemisphere. (C) Confocal image of a coronal section showing the expression pattern surrounding the injection site (asterisk) in a different brain together with NeuN counterstain. Dense YC3.60 labeling of cortical neurons is observed preferentially in L2/3 and L5. (D) A magnified view on the neocortical layers reveals that a large fraction of neurons (red) in L2/3 is also labeled with YC3.60. (E, F) Two-photon images of YFP fluorescence in fixed brain slices showing YC3.60 labeling of somata excluding the nucleus as well as of dendrites in L2/3 and in L5 neurons, respectively.

Three weeks or longer after stereotactic virus injection, YC3.60 expression appeared as a bright fluorescent spot with a diameter of 0.5-1 mm (Figure 1B). Analyses of fixed brain slices showed that near the injection site a majority of cortical neurons (>80%) in layer 2/3 (L2/3) and L5 were fluorescently labeled (Figure 1C and 1D). Neurospecificity of YC3.60 expression was confirmed by overlap with NeuN-staining. Cells showed bright

staining in soma excluding the nucleus (Figure 1E and 1F) as reported for other FCIPs (Hasan et al., 2004; Tian et al., 2009; Wallace et al., 2008). Due to the dense expression, the neuropil (including dendrites and axons) was also brightly stained near the injection site. YC3.60-expressing cells could be imaged by two-photon microscopy in the living mouse brain down to about 400  $\mu\text{m}$  covering the supergranular layers (Figure 2A). Vertically running apical dendrites of pyramidal neurons were clearly visible in side projections of image stacks (Figure 2B). In vivo counterstaining with the astrocyte-marker sulforhodamine 101 (SR101) (Nimmerjahn et al., 2004) revealed a complete lack of overlap with YC3.60 staining confirming neurospecificity (Figure 2C).

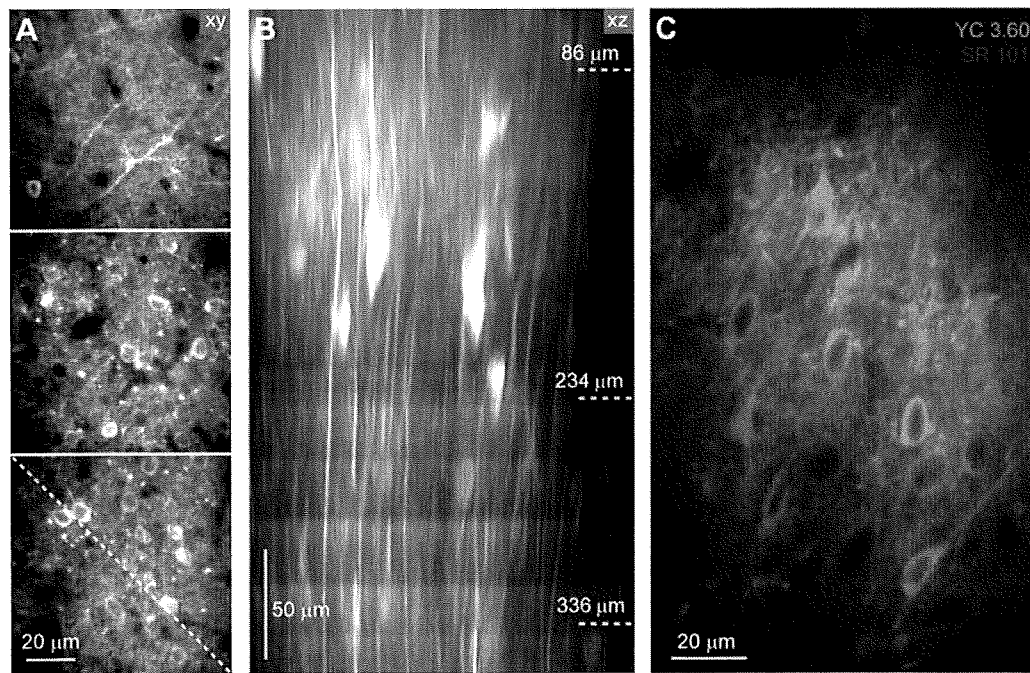


**Figure 2. In vivo imaging of YC3.60-expressing neocortical neurons**

(A) In vivo two-photon image stack of YC3.60-expressing neurons in mouse barrel cortex 4 weeks after AAV-injection. Three example YFP images are shown from superficial L1 (86  $\mu\text{m}$  depth from pia, top), upper L2/3 (234  $\mu\text{m}$  depth, middle) and deeper L2/3 (336  $\mu\text{m}$  depth, bottom). Note labeled horizontal dendrites in L1 and dense labeling of somata in L2/3. (B) Vertically resliced side projection of the image stack in (A) showing apical dendrites of pyramidal neurons. Dashed line in the lower image in (A) indicates the section for vertical z-reslicing. Projection extension was about 20  $\mu\text{m}$ . (C) In vivo two-photon image of neuronal YC3.60 expression (green, YFP channel) together with counterstaining of astrocytes with SR101 (red).

YC3.60 reports increases in intracellular free  $\text{Ca}^{2+}$  concentration as a FRET change caused by a conformational change that brings CFP and YFP closer together (Nagai et al., 2004). The acceptor (YFP) fluorescence intensity is expected to increase while the donor (CFP) fluorescence should decrease. Indeed, YFP-increases and concomitant CFP-decreases were observed in initial experiments on rat organotypic hippocampal slices, in which increasing number of synaptic shocks were delivered to the mossy fibers and

fluorescence changes were recorded in the neuropil of the CA3 region (Figure 3A). Expressed as relative percentage change of the YFP/CFP ratio ( $\Delta R/R$ ), the evoked signals showed a large dynamic range, with peak signals up to 50% and little indication of saturation. AP-evoked calcium transients of smaller amplitude were readily observed in single cells, both in vitro (Figure 3B) and in vivo (Figure 3C). Even though a ratiometric measurement with simultaneous acquisition of fluorescence in the YFP- and CFP-channel is advantageous as it normalizes for common baseline drifts, the relative fluorescence changes in the YFP-channel alone ( $\Delta F/F_{YFP}$ ) also clearly indicated  $Ca^{2+}$  transients (Figure 3B and 3C). In the following sections, we will present  $Ca^{2+}$  transients either as relative percentage change of the ratio YFP/CFP ( $\Delta R/R$ ) or as  $\Delta F/F_{YFP}$ .

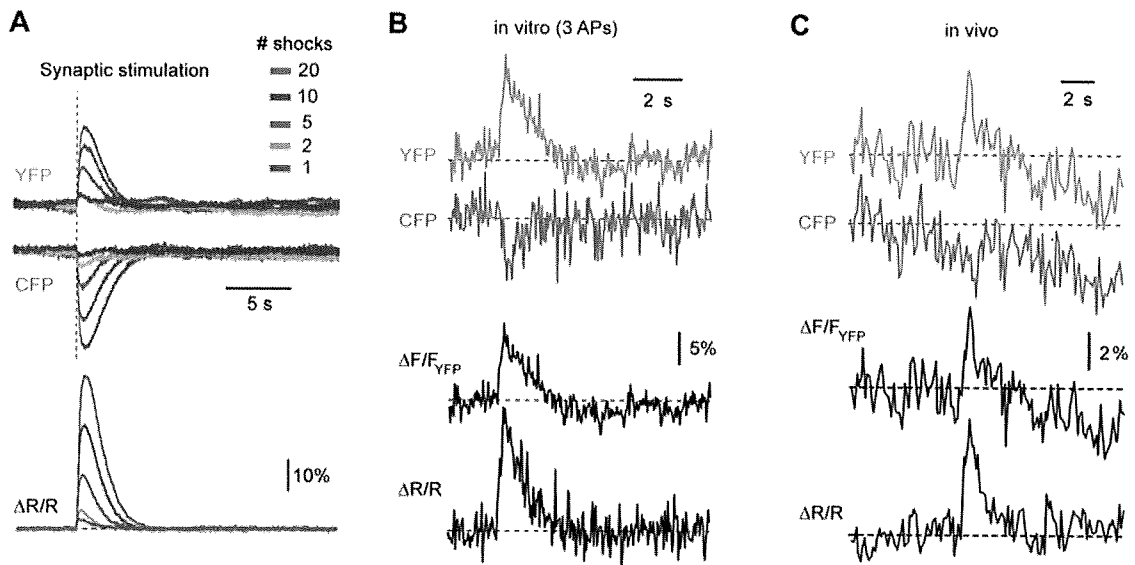


**Figure 3.  $Ca^{2+}$  signals reported by YC3.60**

(A) Two-photon line scan measurements of YC3.60 signals in the neuropil of hippocampal slice cultures. Fluorescence changes were evoked by extracellular stimulation at 100 Hz with different number of stimuli, averaged along the line length and over five stimulus presentations. Top: Fluorescence signals in the YFP and CFP channel (smoothed with a 30-ms window), Bottom: YFP/CFP ratio changes expressed as  $\Delta R/R$  (smoothed with a 100-ms window). Note that intensity increases in the YFP-channel and decreases in the CFP-channel. (B) Example fluorescence transient from an individual YC3.60-expressing hippocampal neuron in vitro following synaptic stimulation, which evoked three action potentials. The  $Ca^{2+}$  transient is expressed either as relative percentage change in the YFP channel ( $\Delta F/F_{YFP}$ ) or as percentage change in the YFP/CFP ratio ( $\Delta R/R$ ). (C) Analogous in vivo example of a spontaneously occurring fluorescence transient in a YC3.60-expressing L2/3 neocortical neuron. In (A)-(C) raw fluorescence intensities of CFP and YFP are reported in arbitrary units.

### 3.2. YC3.60 reports AP firing in vitro and in vivo

We next examined how sensitively YC3.60 reports AP firing in vitro and in vivo by combining targeted electrical recordings with two-photon imaging (see Materials and Methods). Synaptic stimulation of pyramidal neurons in slice cultures elicited single APs or bursts of AP trains as revealed by juxtacellular recordings (Figure 4A). Single APs evoked  $\text{Ca}^{2+}$  transients with an average  $\Delta R/R$  amplitude of  $5.9 \pm 0.3\%$  (mean  $\pm$  S.E.M.,  $n = 32$ ), while high-frequency bursts of 2, 3, and 5 APs elicited successively larger transients ( $10.1 \pm 0.3\%$  (40),  $13.8 \pm 0.4\%$  (35) and  $18.7 \pm 1.1\%$  (4), respectively). The increase in  $\text{Ca}^{2+}$  transient amplitude with number of APs was well approximated by a linear fit (Figure 4C; slope =  $3.15\%/AP$ ;  $r^2 = 0.98$ ). The decay of  $\text{Ca}^{2+}$  transients was relatively fast and did not significantly depend on AP number (Figure 4D; time constants of exponential fits:  $0.78 \pm 0.05$  s,  $0.82 \pm 0.03$  s,  $0.91 \pm 0.04$  s, and  $0.80 \pm 0.06$  s for 1, 2, 3 and 5 APs, respectively; slope of linear regression 4 ms/AP).

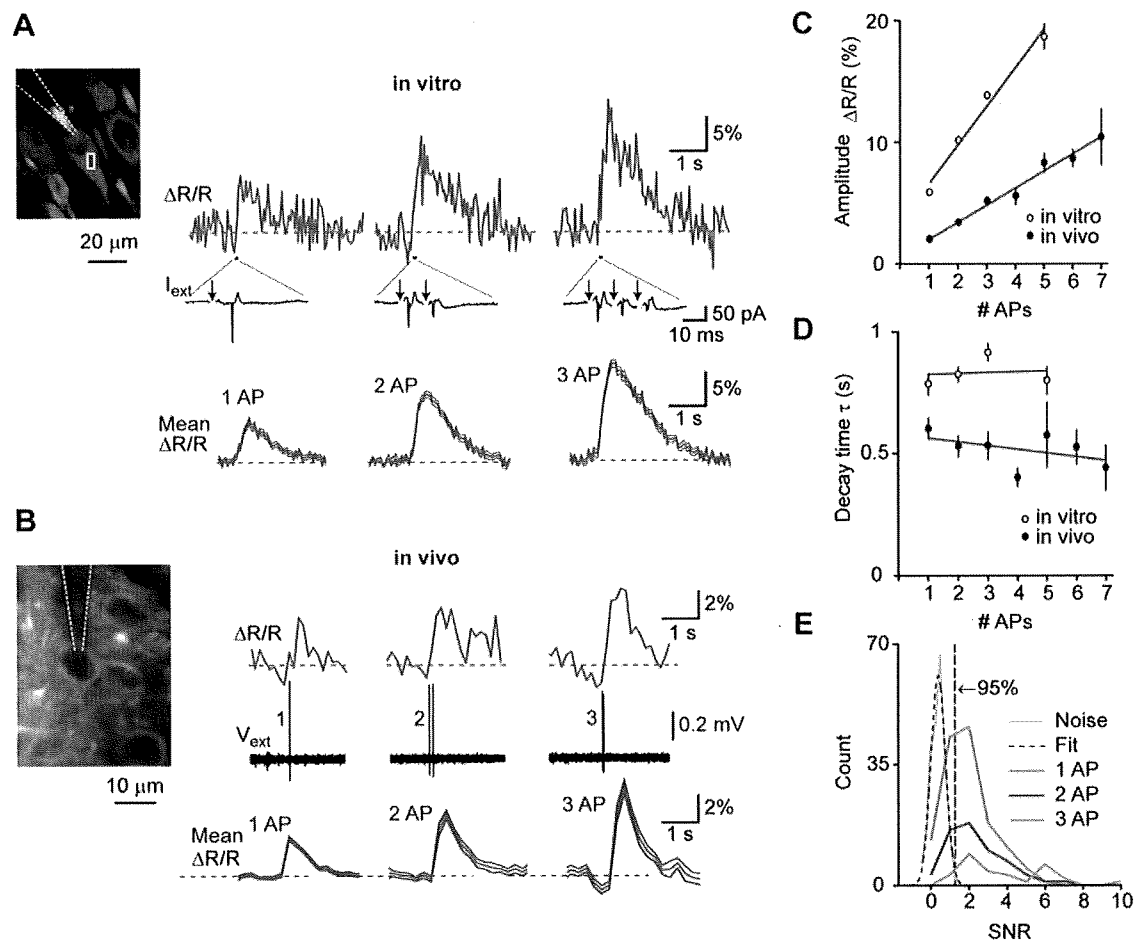


**Figure 4. YC3.60 sensitivity to action potentials in vitro and in vivo**

(A) Characterization of YC3.60 sensitivity in vitro. Top: Cell-attached recording at room temperature from a hippocampal CA3 pyramidal neuron (left image with recording pipette) and simultaneous fluorescence measurement from a somatic region of interest (white box). Extracellular current and single-trial  $\text{Ca}^{2+}$  transients are shown in response to 1, 2 and 3 APs elicited by synaptic stimulation (arrows; stimulation pipette not shown;

stimulus artifacts blanked). Bottom: Mean fluorescence traces ( $\pm$ S.E.M.) in response to 1, 2 and 3 APs ( $n = 32$  traces from 4 cells for 1 AP;  $n = 40$  (5) for 2 APs;  $n = 35$  (5) for 3 APs). **(B)** Characterization of YC3.60 sensitivity in vivo. Top: Juxtacellular voltage recording from a L2/3 neuron in barrel cortex (left image with recording pipette) and simultaneous two-photon  $\text{Ca}^{2+}$  measurement from the soma region. Example  $\text{Ca}^{2+}$  transients are shown for spontaneously occurring 1, 2 and 3 APs. Bottom: Mean fluorescence traces ( $\pm$ S.E.M.) in response to 1, 2 and 3 APs ( $n = 78$  traces from 9 cells for 1 AP;  $n = 33$  (7) for 2 APs;  $n = 23$  (7) for 3 APs). **(C)** Peak amplitudes of  $\text{Ca}^{2+}$  transients as a function of number of APs (in vitro, open circles,  $n = 32, 40, 35$  and 4 transients for 1, 2, 3 and 5 APs, respectively; in vivo, filled circles,  $n = 138$  transients from 11 cells, 61 (9), 30 (9), 18 (7), 12 (6), 4 (3), 6 (5) for 1-7 APs, respectively). **(D)** Decay time constants of exponential fits as a function of number of APs (in vitro, open circles, same  $n$  as in C; in vivo, filled circles  $n = 78$  (9), 33 (7), 23 (7), 16 (6), 11 (5), 3 (2), 5 (5) for 1-7 APs, respectively). Red lines are linear regressions. Error bars are shown as S.E.M. **(E)** Efficiency of AP detection in vivo was determined by estimating the distribution of the signal to noise ratio (SNR) under noise conditions (solid blue) and fitting with a Gaussian (broken blue). From the fit, we determined the SNR cutoff at which less than 5% of baseline traces would be classified as false positives (SNR = 1.3). Using this threshold, 71% of single APs (97 / 137), 80% of doublets (48 / 60) and 93% of triplets (27 / 29) were correctly detected.

To determine YC3.60 sensitivity in vivo, we performed two-photon targeted juxtacellular recordings from YC3.60-expressing L2/3 neurons in barrel cortex of anesthetized mice (Figure 4B). In many cases, single APs were associated with clear  $\Delta R/R$  transients. On average, single APs elicited transients of  $2.00 \pm 0.09\%$  peak amplitude ( $n = 138$  transients from 11 cells). Bursts of up to 7 APs elicited transients with successively larger amplitude (Figure 4C). The relationship between  $\text{Ca}^{2+}$  transient amplitude and AP number again was well approximated by a linear fit (slope =  $1.39\%/AP$ ;  $r^2 = 0.98$ ), indicating that YC3.60 fluorescence changes for bursts of APs were well below saturation. Indeed, much larger events (20–30%  $\Delta R/R$ ) were occasionally observed in response to trains of 10 or more APs (see Figure 5B). We estimated AP-detection efficiency by comparing the signal-to-noise ratio of AP-evoked transients to the baseline noise level (see Materials and Methods). Detection rates were 71% for single APs and 80% and 93% for bursts of 2 and 3 APs, respectively (Figure 4E). Similar to the in vitro results,  $\text{Ca}^{2+}$  transients showed fast decays, which did not depend on AP number (Figure 4D; for single APs  $0.60 \pm 0.05$  s;  $n = 78$  transients from 9 cells; slope of linear regression -16 ms/AP). The differences in absolute values for peak amplitudes and decay time constants between in vitro and in vivo experiments most likely can be attributed to the differences in experimental conditions. In particular, a similar reduction of AP-evoked  $\text{Ca}^{2+}$  transient amplitude at physiological compared to room temperature has also been reported for other FCIPs (Mao et al., 2008; Tian et al., 2009). We conclude that YC3.60 sensitively reports AP firing both in vitro and in vivo and that it can even resolve single APs.

### 3.3. Sensory-evoked and spontaneous subcellular, cellular and wide-field $\text{Ca}^{2+}$ signals

We next investigated in how far YC3.60 can be used to study sensory-evoked cortical activity on various spatial scales, ranging from dendrites of individual neurons to large areas of the barrel field. On the finest scale, we simultaneously measured spontaneous dendritic and somatic  $\text{Ca}^{2+}$  transients in L2/3 pyramidal neurons using ‘arbitrary plane’ imaging (Göbel and Helmchen, 2007b) (Figure 5A). As expected (Schiller et al., 1995),  $\text{Ca}^{2+}$  transients showed faster decay times in apical dendrites compared to somata ( $0.35 \pm 0.04$  s vs.  $0.47 \pm 0.04$  ms;  $n = 23$ ;  $p < 0.01$ ; paired 2-tailed t-test), confirming relatively rapid kinetics of YC3.60. A large dynamic range of YC3.60 is demonstrated in Figure 5B, where  $\text{Ca}^{2+}$  transients evoked by complex AP patterns (ranging from individual APs to trains of 10 or more APs) were revealed with high fidelity. The peak  $\Delta R/R$  amplitudes of around 30% in these recordings presumably still are far from indicator saturation (see Figure 3A).

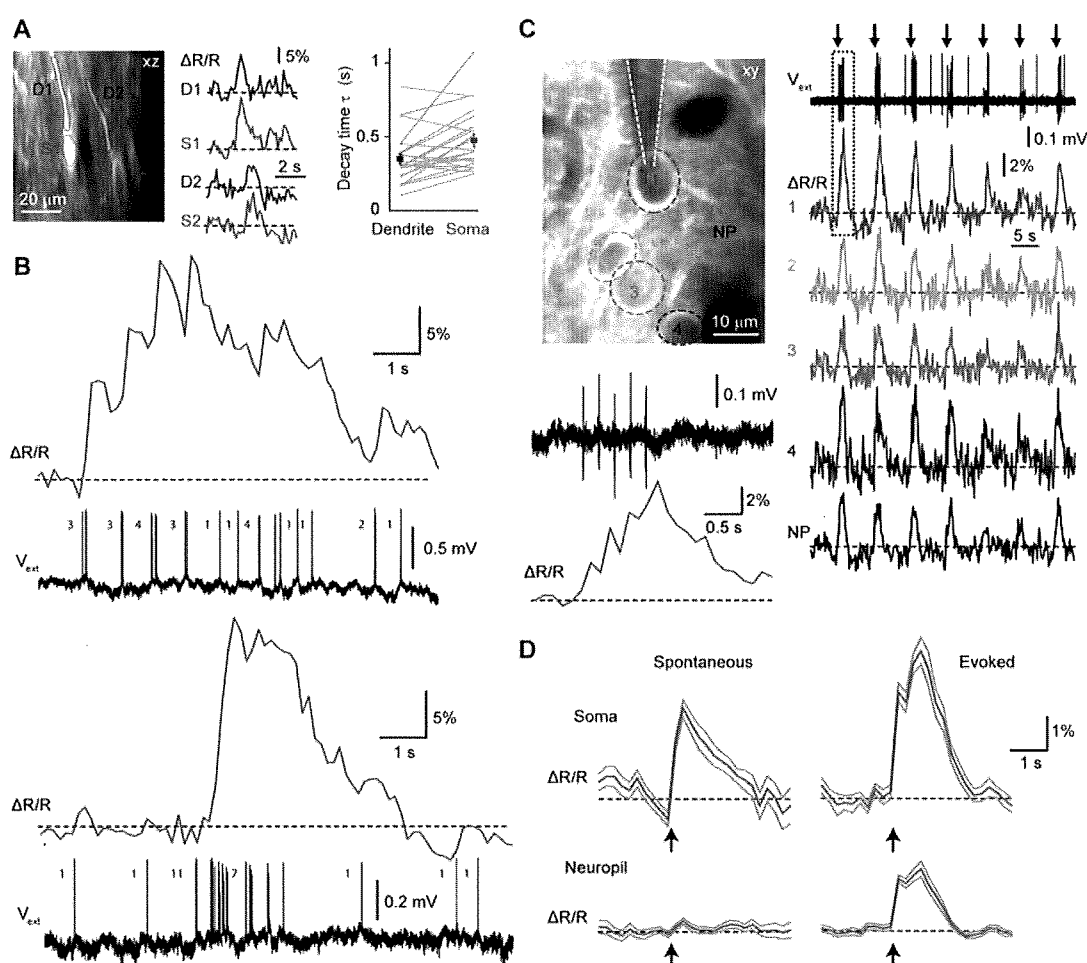


**Figure 5. Single-cell and population YC3.60  $\text{Ca}^{2+}$  signals in L2/3 of barrel cortex**  
 (A) Simultaneous two-photon  $\text{Ca}^{2+}$  imaging in soma and dendrites of L2/3 neurons using vertical (xz-)imaging. Examples of spontaneous somatic (S, red) and apical dendritic (D, blue) YC3.60  $\text{Ca}^{2+}$  transients for the cells depicted in the left image. Right: Mean decay times in dendrites compared to somata for 23 measurements (grey lines; mean $\pm$ S.E.M).

**(B)** Simultaneous juxtacellular voltage recording and two-photon  $\text{Ca}^{2+}$  imaging from a neuron showing rare events of sustained and high-frequency AP firing in L2/3 neurons that are accompanied by large YC3.60  $\text{Ca}^{2+}$  transients with peak amplitudes of up to 30%  $\Delta\text{R/R}$ . Top: Sustained AP firing leads to prolonged elevation of the fluorescence ratio. Bottom: A short burst of 11 APs is accompanied by a fast  $\text{Ca}^{2+}$  transient, which returns to baseline following a stereotypical exponential decay. **(C)** Two-photon  $\text{Ca}^{2+}$  imaging of a small population of neurons during sensory stimulation (seven times 5 air-puffs to contralateral whiskers at 5 Hz). Large  $\text{Ca}^{2+}$  transients in cell 1 (red trace) correlated with the spiking activity observed in the simultaneous juxtacellular voltage recording. Concomitant  $\text{Ca}^{2+}$  transients were also evoked in neighboring neuronal somata and in the nearby neuropil (NP). The response to the first stimulation episode (dashed box) is shown on expanded scale in the lower left, indicating that YC3.60 resolves the individual steps in the accumulated  $\text{Ca}^{2+}$  response. **(D)** Event-triggered average  $\text{Ca}^{2+}$  traces from somata and adjacent neuropil for spontaneous ( $n = 37$  events of 1–3 APs) and evoked ( $n = 32$  events of 1–5 APs) action potentials. Multi-whisker air puff-evoked  $\text{Ca}^{2+}$  transients in somata were significantly larger than those in the neuropil while spontaneous spikes were accompanied by somatic but no neuropil transients. Errors are shown as S.E.M.

On the level of local neuronal populations, air-puff whisker stimulation (5 Hz) elicited clear  $\text{Ca}^{2+}$  transients in neuronal somata but also in the neuropil (Figure 5C). Bursts of AP firing could be distinguished even at relatively slow frame rates (7.81 Hz), highlighting the rapid kinetics of the  $\text{Ca}^{2+}$  sensor. Combined electrical recordings allowed to directly assess the degree of potential contamination of somatic signals by  $\text{Ca}^{2+}$  signals in the surrounding neuropil (Göbel and Helmchen, 2007a; Kerr et al., 2005). Whisker-evoked events were associated with significantly larger  $\text{Ca}^{2+}$  transients in somata compared to the neighboring neuropil ( $4.0 \pm 0.5$  vs.  $1.6 \pm 0.2\%$   $\Delta\text{R/R}$ ,  $n = 32$ ,  $p < 0.01$ , paired 2-tailed t-test). In contrast, spontaneously occurring APs elicited  $\text{Ca}^{2+}$  transients in somata but not in the neuropil ( $2.3 \pm 0.4\%$  vs.  $0.4 \pm 0.1\%$ ,  $n = 37$ ,  $p < 0.01$ ). (Figure 5D-E). From these observations we conclude that sensory stimulation can evoke  $\text{Ca}^{2+}$  transients in the neuropil in addition to somatic signals, presumably reflecting excitation of afferent axonal pathways (Kerr et al., 2005), but that high-resolution two-photon imaging clearly distinguishes the cellular AP-evoked signals.

Activation of a substantial fraction of neurons in the local population as well as of the surrounding neuropil might cause sufficient YC3.60 signals for large-scale bulk recording of barrel cortex excitation. Indeed, in addition to sensory-evoked responses spontaneous fluctuating calcium signals were apparent in the neuropil when entire two-photon imaging frames were used as ROI (Figure 6A). Similar spontaneous YC3.60 signals were observed with wide-field single-photon-excited fluorescence with a CCD-camera positioned above barrel cortex (Figure 6B). These slow oscillations closely corresponded to the simultaneously measured local field potential (LFP) and most likely are due to synchronous activity during anesthesia. In addition, air puff stimulation of whiskers evoked stimulus-locked LFP signals and bulk fluorescence changes with an average  $\Delta\text{F}/\text{F}_{\text{YFP}}$  amplitude of  $0.47 \pm 0.03\%$  and an average decay time of  $0.48 \pm 0.04$  s ( $n = 3$  animals). Bulk-activity in barrel cortex could also be read out using single-photon excitation and fluorescence collection through a single-core optical fiber (440  $\mu\text{m}$  core

diameter; see Material and Methods). With the optical fiber placed on top of the dura (or the thinned skull) of anesthetized mice showing YC3.60 expression in barrel cortex, we observed both spontaneous and air puff-evoked  $\Delta F/F_{YFP}$  signals (Figure 6C) that were similar to the signals observed by wide-field camera imaging.

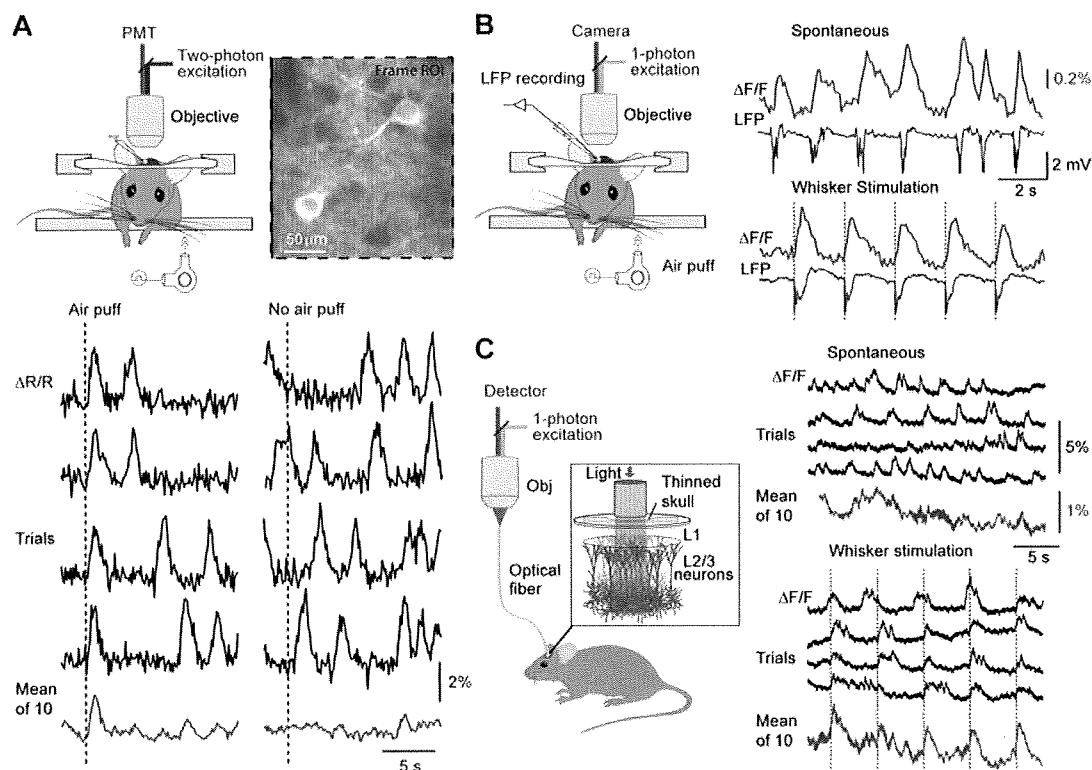


**Figure 6. Bulk recording of spontaneous and sensory-evoked YC3.60  $Ca^{2+}$  signals in barrel cortex**

(A) Large-area  $Ca^{2+}$  imaging using two-photon excitation and whisker stimulation by air puffs. Neuropil and two neurons visible about 100  $\mu m$  deep in a 12-week-old mouse ~6 weeks after virus infection. The entire frame was taken as region of interest. Bottom: Examples of single-trial spontaneous and sensory-evoked responses are shown along with average traces of 10 trials. (B) Large-area  $Ca^{2+}$  imaging using single-photon excitation and a camera and simultaneous local-field potential recording (LFP) in barrel cortex of an anesthetized mouse (left schematic). Right: The mean YC3.60 fluorescence signal ( $\Delta F/F$  in YFP-channel; red traces) correlated well with the LFP for both spontaneous activity (top) and upon air-puff whisker stimulation (bottom; dashed vertical lines). (C) Fiber-optic bulk recording of YC3.60 signals in barrel cortex in an anesthetized mouse (left schematic). Fluorescence excitation and detection were both accomplished through the optical fiber, the tip of which was placed on the cortical surface. Right: Examples of single-trial YC3.60 fluorescence traces ( $\Delta F/F$  in YFP-channel) and mean of 10 traces for spontaneous activity (top) and upon air-puff whisker stimulation (bottom; dashed vertical lines).



### 3.4. Fiber-optic recording of barrel cortex activity in freely moving mice

Fiber-optic recordings enable measurements of neuronal activity in awake, freely behaving animals (Adelsberger et al., 2005; Murayama and Larkum, 2009b; Murayama et al., 2007; for review see Grewe and Helmchen, 2009; Wilt et al., 2009). We tested if YC3.60 expression is suitable for such an application. Using firm attachment of the single optical fiber to the animal's head (Murayama and Larkum, 2009b) we measured bulk fluorescence from the barrel field in awake, freely moving mice (Figure 7). While the mice were either passively sitting or actively exploring, we recorded complex  $\Delta F/F_{YFP}$  signals (Figure 7A-C). We could block the  $Ca^{2+}$  transients by application of  $Cd^{2+}$ , a  $Ca^{2+}$  channel blocker, to the cortical surface (Figure 7D), indicating that the YC3.60 sensor was reporting  $Ca^{2+}$  transients. Mechanically jolting the fiber did not result in obvious fluorescence changes in YC3.60-expressing mice as in previous fiber-optic studies (Murayama and Larkum, 2009b; Murayama et al., 2007). Furthermore, fluorescence traces in a wild-type mouse (without YC3.60) were flat without any movement-related changes (Figure 7E). Together these findings exclude opto-mechanical artifacts as source of the observed fluorescence changes and instead indicate that YC3.60 signals are caused by  $Ca^{2+}$  channel activation and thus provide a readout of the complex activation pattern in the barrel cortex. Fiber-optic recordings using YC3.60 thus should permit closer investigation of behavioral-related activity in specific neocortical areas.

## 4. Discussion

In vivo  $Ca^{2+}$  imaging in the mammalian neocortex so far mainly relied on synthetic indicator dyes (Garaschuk et al., 2006; Gobel and Helmchen, 2007a; Grewe and Helmchen, 2009; Kerr and Denk, 2008). Recently, different FCIPs (also called genetically encoded  $Ca^{2+}$  indicators or GECIs) have been developed that will allow for a more specific interrogation of various aspects of neural activity, compared to synthetic sensors. Here, we have shown that upon neuron-specific expression in the mouse neocortex, the FCIP, YC3.60, can be used to read out activation of neocortical areas at different spatial scales both in anaesthetized and awake, freely moving animals.

Original characterization of YC3.60 (Nagai et al., 2004) defined it as an indicator with high sensitivity and dynamic range in vitro. However, reliable  $Ca^{2+}$  imaging in vivo was not demonstrated in transgenic animals (Nagai et al., 2004), possibly due to the use of a plasma-membrane bound version of the sensor which may have resulted in a reduced AP detection efficiency (Mao et al., 2008). Subsequently, YC3.60 was employed to obtain quantitative  $Ca^{2+}$  concentration measurements in brain slices (Liu et al., 2008) and resting  $Ca^{2+}$  concentrations in vivo (Kuchibhotla et al., 2008). The current study extends these findings by demonstrating that viral delivery of YC3.60 permits in vivo measurements of sensory-evoked  $Ca^{2+}$  signals that closely correspond to cellular AP firing patterns. Furthermore, we have shown that YC3.60 can be applied to monitor neural activity at diverse spatial scales, covering dendritic  $Ca^{2+}$  signals, AP firing in local neuronal populations as well as large scale brain areas.

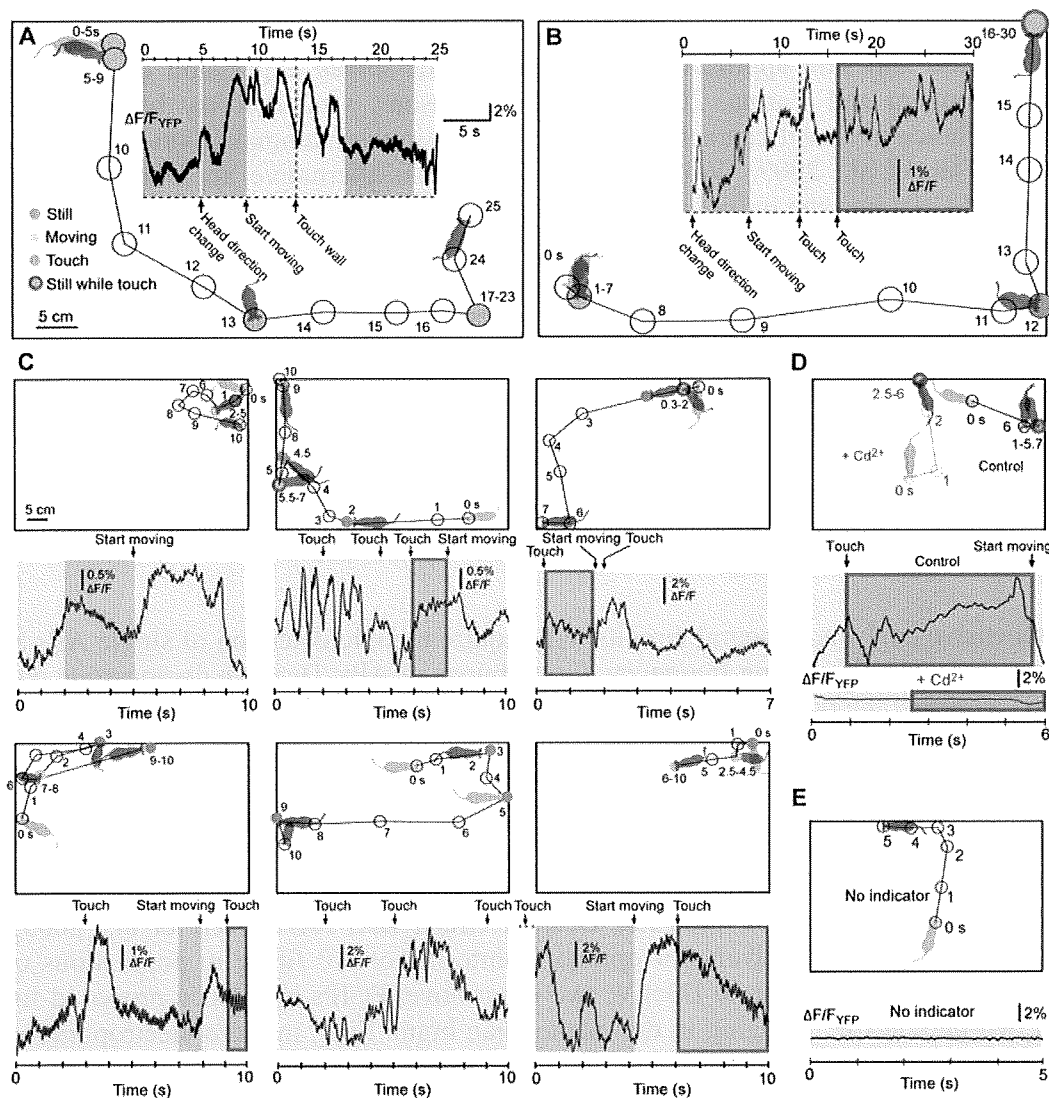


**Figure 7. Fiber-optic recording of brain area activity in freely moving mice using YC3.60.**

(A and B) Two examples of fiber-optic recording of YC3.60 signals in awake, freely moving mice. Bulk  $\text{Ca}^{2+}$  signals indicating neuronal activity were recorded in somatosensory cortex through a single-core optical fiber as shown in Fig. 6C. Fluorescence changes in the YFP-channel are shown during 25-30 s periods together with the position of the mouse in an open field box. Animal behavior (sitting still, moving, touches, or having contact to the wall) is indicated by background colors. The trajectory of the animals' movement is indicated with selected time stamps. (C) Six more examples of  $\text{Ca}^{2+}$  imaging from 3 mice, together with corresponding behavioral observations. Changes of the animal's behavioral state (e.g. start of movement) were frequently associated with marked discontinuities in the fluorescence trace, indicating complex underlying  $\text{Ca}^{2+}$  dynamics. (D) Control experiment showing that  $\text{Ca}^{2+}$  signals are blocked by local perfusion of the cortical region with  $\text{Cd}^{2+}$ . (E) Control experiment demonstrating that a flat fluorescence trace is observed in the absence of YC3.60 expression.

Gene delivery by AAV-vectors (Zhu et al., 2007) provides a highly flexible, straightforward and safe approach for dense and wide-spread expression of FCIPs in neurons (Kootstra and Verma, 2003). For these reasons, viral delivery has been the method of choice in recent characterizations of FCIPs in the mammalian brain (Mank et al., 2008; Tian et al., 2009; Wallace et al., 2008). An alternative approach for gene delivery of FCIPs into the brain is in utero electroporation, which provides the potential benefit of cell-type specificity, depending on the precise electroporation protocol (Borrell et al., 2005) but which results in relatively sparse labeling of neurons compared to viral delivery (Mank et al., 2008). Finally, the production of transgenic mice expressing a number of different FCIPs has been reported (Hasan et al., 2004; Heim et al., 2007) including membrane-bound YC3.60 (Nagai et al., 2004). In one of these studies, sensory-evoked  $\text{Ca}^{2+}$  transients were demonstrated using wide-field imaging of the olfactory bulb with two FCIPs expressed under a tetracycline-inducible promoter (Hasan et al., 2004). The widespread use of these mouse lines has been limited, however, by the failure to clearly monitor AP-evoked cellular  $\text{Ca}^{2+}$  signals in vivo, possibly due to low protein expression levels.

Comprehensive analysis of neural circuits will require reliable detection of single APs as well as estimation of the firing frequency during bursts of APs. Here we demonstrate that YC3.60 can detect the occurrence of single APs in pyramidal cells of mouse barrel cortex in vivo with a sensitivity comparable to recent reports of another ratiometric FCIP, D3cpV (Wallace et al., 2008). Unlike D3cpV, however, YC3.60 shows faster kinetics and minimal saturation for bursts of up to at least 10 APs, thus making it a suitable tool for quantitative investigation of local neural network dynamics in vivo. Overall our analysis revealed that YC3.60 shows comparable signals in terms of sensitivity and decay times to the commonly used synthetic indicator Oregon Green BAPTA-1 (Kerr et al., 2005), which has been used extensively for optical monitoring of AP firing in populations of neurons. Recently, in addition to D3cpV, two other novel FCIPs have been proposed for in vivo two-photon  $\text{Ca}^{2+}$  imaging in the mammalian brain. First, in utero electroporation of TN-XXL, a troponin-based ratiometric FCIP, allowed repeated  $\text{Ca}^{2+}$  imaging from the same neurons over days; however its sensitivity to AP firing was relatively low with single AP detection only achievable in brain slices (Mank et al., 2008). Second, AAV-delivery of the single-fluorescent protein sensor GCaMP-3 has recently been shown to exhibit large fluorescence changes and to detect APs with fast kinetics and little saturation in mouse somatosensory cortex in vivo (Tian et al., 2009). This  $\text{Ca}^{2+}$  sensor does not, however, permit ratiometric imaging and thus will be more susceptible to motion artifacts compared to YC3.60. It is likely that in the near future improved versions of either cameleons or GCaMPs will provide even better optical readout of neuronal spiking. Furthermore, single-fluorophore FCIPs may be co-expressed with a second indicator that is not  $\text{Ca}^{2+}$ -sensitive in order to reduce their susceptibility to motion artifacts.

In addition to two-photon  $\text{Ca}^{2+}$  imaging at the level of single cells and small populations of neurons, we demonstrated the use of FCIPs to record large-scale neuronal activity in awake, freely moving animals. Using a fiber-optic approach (Murayama and Larkum, 2009b; Murayama et al., 2007) to image bulk neural activity in mouse barrel cortex, we

showed complex  $\text{Ca}^{2+}$  dynamics associated with behaviorally salient events such as object-touching or moving. We suggest that these activity patterns may reflect the dynamic interaction of different behavior-related brain states with sensory-evoked activity.

In conclusion, viral delivery of YC3.60 provides a powerful tool for the optical interrogation of neural circuits at multiple spatial scales and with high sensitivity. Viral delivery of FCIPs may in the future be combined with the powerful tools of mouse genetics, allowing for cell-type specific or inducible expression of  $\text{Ca}^{2+}$  sensors (Wallace et al., 2008; Zhu et al., 2007). Thus, injection of AAV-FCIP vectors with loxP sites (Atasoy et al., 2008; Kuhlman and Huang, 2008) into Cre driver mouse lines should allow selective expression of YC3.60 in specific cortical layers (Madisen et al.) and interneuron subtypes (Chattopadhyaya et al., 2004; Oliva et al., 2000). Cell-type specific expression, combined with fiber optic recordings in freely moving animals, will allow functional correlation of specific neuronal populations with behavior. Moreover, the approach developed here may conceivably be adapted to other mammalian species, such as rats (Foti et al., 2007) or even non-human primates (Stettler et al., 2006) and is therefore likely to play an important role in the dissection of the neural underpinnings of complex behaviors.

### Acknowledgments

We like to thank Winfried Denk and Peter H. Seeburg for generous support and interest in the project, and Andreas Schaefer for supporting T.H. We also thank Erika Heil for art work (Art for Biomed, Frankfurt, Germany) and Matthias Heindorf for help on plots. This work was supported by the Max Planck Society, Collaborative Research Grant (SFB636/A4), Volkswagen foundation (AZ: I/80 704) to R.S., a grant from the Swiss National Science Foundation (#3100A0-114624) to F.H., a grant from the Swiss Systems Biology Initiative SystemsX.ch to F.H. and M.L. (Neurochoice project), the German Academic Exchange Service (DAAD) to H.L., the Sumitomo Foundation and Research Foundation for Opto-Science and Technology to M.M., and Schloessmann Foundation and Fritz Thyssen Stiftung to M.T.H.

### References

- Adelsberger, H., Garaschuk, O., and Konnerth, A. (2005). Cortical calcium waves in resting newborn mice. *Nat Neurosci* 8, 988-990.
- Atasoy, D., Aponte, Y., Su, H.H., and Sternson, S.M. (2008). A FLEX switch targets Channelrhodopsin-2 to multiple cell types for imaging and long-range circuit mapping. *J Neurosci* 28, 7025-7030.
- Berger, T., Borgdorff, A., Crochet, S., Neubauer, F.B., Lefort, S., Fauvet, B., Ferezou, I., Carleton, A., Lüscher, H.R., and Petersen, C.C. (2007). Combined voltage and calcium epifluorescence imaging in vitro and in vivo reveals subthreshold and suprathreshold dynamics of mouse barrel cortex. *J Neurophysiol* 97, 3751-3762.
- Borrell, V., Yoshimura, Y., and Callaway, E.M. (2005). Targeted gene delivery to telencephalic inhibitory neurons by directional in utero electroporation. *J Neurosci Methods* 143, 151-158.

- Chattopadhyaya, B., Di Cristo, G., Higashiyama, H., Knott, G.W., Kuhlman, S.J., Welker, E., and Huang, Z.J. (2004). Experience and activity-dependent maturation of perisomatic GABAergic innervation in primary visual cortex during a postnatal critical period. *J Neurosci* 24, 9598-9611.
- Foti, S., Haberman, R.P., Samulski, R.J., and McCown, T.J. (2007). Adeno-associated virus-mediated expression and constitutive secretion of NPY or NPY13-36 suppresses seizure activity in vivo. *Gene therapy* 14, 1534-1536.
- Garaschuk, O., Milos, R.I., and Konnerth, A. (2006). Targeted bulk-loading of fluorescent indicators for two-photon brain imaging in vivo. *Nat Protoc* 1, 380-386.
- Göbel, W., and Helmchen, F. (2007a). In vivo calcium imaging of neural network function. *Physiology (Bethesda)* 22, 358-365.
- Göbel, W., and Helmchen, F. (2007b). New angles on neuronal dendrites in vivo. *J Neurophysiol* 98, 3770-3779.
- Grewe, B.F., and Helmchen, F. (2009). Optical probing of neuronal ensemble activity. *Curr Opin Neurobiol*.
- Hasan, M.T., Friedrich, R.W., Euler, T., Larkum, M.E., Giese, G., Both, M., Duebel, J., Waters, J., Bujard, H., Griesbeck, O., *et al.* (2004). Functional fluorescent  $\text{Ca}^{2+}$  indicator proteins in transgenic mice under TET control. *PLoS Biol* 2, e163.
- Heim, N., Garaschuk, O., Friedrich, M.W., Mank, M., Milos, R.I., Kovalechuk, Y., Konnerth, A., and Griesbeck, O. (2007). Improved calcium imaging in transgenic mice expressing a troponin C-based biosensor. *Nat Methods* 4, 127-129.
- Helmchen, F., and Denk, W. (2005). Deep tissue two-photon microscopy. *Nat Methods* 2, 932-940.
- Helmchen, F., Imoto, K., and Sakmann, B. (1996).  $\text{Ca}^{2+}$  buffering and action potential-evoked  $\text{Ca}^{2+}$  signaling in dendrites of pyramidal neurons. *Biophys J* 70, 1069-1081.
- Helmchen, F., Svoboda, K., Denk, W., and Tank, D.W. (1999). In vivo dendritic calcium dynamics in deep-layer cortical pyramidal neurons. *Nat Neurosci* 2, 989-996.
- Hires, S.A., Tian, L., and Looger, L.L. (2008). Reporting neural activity with genetically encoded calcium indicators. *Brain Cell Biol* 36, 69-86.
- Kerr, J.N., de Kock, C.P., Greenberg, D.S., Bruno, R.M., Sakmann, B., and Helmchen, F. (2007). Spatial organization of neuronal population responses in layer 2/3 of rat barrel cortex. *J Neurosci* 27, 13316-13328.
- Kerr, J.N., and Denk, W. (2008). Imaging in vivo: watching the brain in action. *Nat Rev Neurosci* 9, 195-205.
- Kerr, J.N., Greenberg, D., and Helmchen, F. (2005). Imaging input and output of neocortical networks in vivo. *Proc Natl Acad Sci U S A* 102, 14063-14068.
- Kootstra, N.A., and Verma, I.M. (2003). Gene therapy with viral vectors. *Annu Rev Pharmacol Toxicol* 43, 413-439.
- Kuchibhotla, K.V., Goldman, S.T., Lattarulo, C.R., Wu, H.-Y., Hyman, B.T., and Bacskaï, B.J. (2008). Abeta plaques lead to aberrant regulation of calcium homeostasis in vivo resulting in structural and functional disruption of neuronal networks. *Neuron* 59, 214-225.
- Kügler, S., Hahnewald, R., Garrido, M., and Reiss, J. (2007). Long-term rescue of a lethal inherited disease by adeno-associated virus-mediated gene transfer in a mouse model of molybdenum-cofactor deficiency. *Am J Hum Genet* 80, 291-297.

- Kuhlman, S.J., and Huang, Z.J. (2008). High-resolution labeling and functional manipulation of specific neuron types in mouse brain by Cre-activated viral gene expression. *PloS one* 3, e2005.
- Liu, X., Gong, H., Li, X., and Zhou, W. (2008). Monitoring calcium concentration in neurons with cameleon. *J Biosci Bioeng* 105, 106-109.
- Madisen, L., Zwingman, T.A., Sunkin, S.M., Oh, S.W., Zariwala, H.A., Gu, H., Ng, L.L., Palmiter, R.D., Hawrylycz, M.J., Jones, A.R., *et al.* A robust and high-throughput Cre reporting and characterization system for the whole mouse brain. *Nat Neurosci* 13, 133-140.
- Mank, M., and Griesbeck, O. (2008). Genetically encoded calcium indicators. *Chem Rev* 108, 1550-1564.
- Mank, M., Santos, A.F., Drenth, S., Mrcic-Flogel, T.D., Hofer, S.B., Stein, V., Hendel, T., Reiff, D.F., Levelt, C., Borst, A., *et al.* (2008). A genetically encoded calcium indicator for chronic in vivo two-photon imaging. *Nat Methods* 5, 805-811.
- Mao, T., O'Connor, D.H., Scheuss, V., Nakai, J., and Svoboda, K. (2008). Characterization and subcellular targeting of GCaMP-type genetically-encoded calcium indicators. *PLoS ONE* 3, e1796.
- Markram, H., and Sakmann, B. (1994). Calcium transients in dendrites of neocortical neurons evoked by single subthreshold excitatory postsynaptic potentials via low-voltage-activated calcium channels. *Proc Natl Acad Sci U S A* 91, 5207-5211.
- Mastakov, M.Y., Baer, K., Xu, R., Fitzsimons, H., and During, M.J. (2001). Combined injection of rAAV with mannitol enhances gene expression in the rat brain. *Mol Ther* 3, 225-232.
- Miyawaki, A., Llopis, J., Heim, R., McCaffery, J.M., Adams, J.A., Ikura, M., and Tsien, R.Y. (1997). Fluorescent indicators for  $\text{Ca}^{2+}$  based on green fluorescent proteins and calmodulin. *Nature* 388, 882-887.
- Miyawaki, A., Nagai, T., and Mizuno, H. (2005). Engineering fluorescent proteins. *Adv Biochem Eng Biotechnol* 95, 1-15.
- Murayama, M., and Larkum, M.E. (2009a). Enhanced dendritic activity in awake rats. *Proc Natl Acad Sci U S A* 106, 20482-20486.
- Murayama, M., and Larkum, M.E. (2009b). In vivo dendritic calcium imaging with a fiberoptic periscope system. *Nat Protoc* 4, 1551-1559.
- Murayama, M., Perez-Garci, E., Lüscher, H.R., and Larkum, M.E. (2007). Fiberoptic system for recording dendritic calcium signals in layer 5 neocortical pyramidal cells in freely moving rats. *J Neurophysiol* 98, 1791-1805.
- Murayama, M., Perez-Garci, E., Nevian, T., Bock, T., Senn, W., and Larkum, M.E. (2009). Dendritic encoding of sensory stimuli controlled by deep cortical interneurons. *Nature* 457, 1137-1141.
- Nagai, T., Yamada, S., Tominaga, T., Ichikawa, M., and Miyawaki, A. (2004). Expanded dynamic range of fluorescent indicators for  $\text{Ca}^{2+}$  by circularly permuted yellow fluorescent proteins. *Proc Natl Acad Sci U S A* 101, 10554-10559.
- Nimmerjahn, A., Kirchhoff, F., Kerr, J.N., and Helmchen, F. (2004). Sulforhodamine 101 as a specific marker of astroglia in the neocortex in vivo. *Nat Methods* 1, 31-37.
- Oliva, A.A., Jr., Jiang, M., Lam, T., Smith, K.L., and Swann, J.W. (2000). Novel hippocampal interneuronal subtypes identified using transgenic mice that express green fluorescent protein in GABAergic interneurons. *J Neurosci* 20, 3354-3368.

- Palmer, A.E., Giacomello, M., Kortemme, T., Hires, S.A., Lev-Ram, V., Baker, D., and Tsien, R.Y. (2006).  $\text{Ca}^{2+}$  indicators based on computationally redesigned calmodulin-peptide pairs. *Chem Biol* 13, 521-530.
- Palmer, A.E., and Tsien, R.Y. (2006). Measuring calcium signaling using genetically targetable fluorescent indicators. *Nat Protoc* 1, 1057-1065.
- Sato, T.R., Gray, N.W., Mainen, Z.F., and Svoboda, K. (2007). The Functional Microarchitecture of the Mouse Barrel Cortex. *PLoS Biol* 5, e189.
- Schiller, J., Helmchen, F., and Sakmann, B. (1995). Spatial profile of dendritic calcium transients evoked by action potentials in rat neocortical pyramidal neurones. *J Physiol* 487 ( Pt 3), 583-600.
- Stettler, D.D., Yamahachi, H., Li, W., Denk, W., and Gilbert, C.D. (2006). Axons and synaptic boutons are highly dynamic in adult visual cortex. *Neuron* 49, 877-887.
- Stoppini, L., Buchs, P.A., and Muller, D. (1991). A simple method for organotypic cultures of nervous tissue. *J Neurosci Methods* 37, 173-182.
- Stosiek, C., Garaschuk, O., Holthoff, K., and Konnerth, A. (2003). In vivo two-photon calcium imaging of neuronal networks. *Proc Natl Acad Sci U S A* 100, 7319-7324.
- Svoboda, K., Denk, W., Kleinfeld, D., and Tank, D.W. (1997). In vivo dendritic calcium dynamics in neocortical pyramidal neurons. *Nature* 385, 161-165.
- Tian, L., Hires, S.A., Mao, T., Huber, D., Chiappe, M.E., Chalasani, S.H., Petreanu, L., Akerboom, J., McKinney, S.A., Schreiter, E.R., *et al.* (2009). Imaging neural activity in worms, flies and mice with improved GCaMP calcium indicators. *Nat Methods* 6, 875-881.
- Wallace, D.J., Zum Alten Borgloh, S.M., Astori, S., Yang, Y., Bausen, M., Kügler, S., Palmer, A.E., Tsien, R.Y., Sprengel, R., Kerr, J.N., *et al.* (2008). Single-spike detection in vitro and in vivo with a genetic  $\text{Ca}^{2+}$  sensor. *Nat Methods* 5, 797-804.
- Waters, J., Larkum, M., Sakmann, B., and Helmchen, F. (2003). Supralinear  $\text{Ca}^{2+}$  influx into dendritic tufts of layer 2/3 neocortical pyramidal neurons in vitro and in vivo. *J Neurosci* 23, 8558-8567.
- Wilt, B.A., Burns, L.D., Wei Ho, E.T., Ghosh, K.K., Mukamel, E.A., and Schnitzer, M.J. (2009). Advances in light microscopy for neuroscience. *Annu Rev Neurosci* 32, 435-506.
- Zhu, P., Aller, M.I., Baron, U., Cambridge, S., Bausen, M., Herb, J., Sawinski, J., Cetin, A., Osten, P., Nelson, M.L., *et al.* (2007). Silencing and un-silencing of tetracycline-controlled genes in neurons. *PLoS ONE* 2, e533.

# **Auto-luminescent Genetically-Encoded Ratiometric Indicator for Real-time $\text{Ca}^{2+}$ Imaging at the Single Cell Level**

Kenta Saito<sup>1</sup>, Noriyuki Hatsugai<sup>1,2</sup>, Kazuki Horikawa<sup>1</sup>, Kentaro Kobayashi<sup>1</sup>, Toru Matsu-ura<sup>3</sup>, Katsuhiko Mikoshiba<sup>3</sup> and Takeharu Nagai<sup>1,4\*</sup>

- 1 Research Institute for Electronic Science, Hokkaido University, Kita-20, Nishi-10 Kita-ku, Sapporo, Hokkaido 001-0020, Japan
- 2 Research Center for Cooperative Projects, Hokkaido University, Kita-15, Nishi-7 Kita-ku, Sapporo, Hokkaido 060-8638, Japan
- 3 RIKEN Brain Science Institute, 2-1 Hirosawa, Wako City, Saitama 351-0198, Japan
- 4 Precursory Research for Embryonic Science, Japan Science and Technology Agency, Sanbancho, Chiyoda-ku, Tokyo 102-0075, Japan

Running title: BRET-based  $\text{Ca}^{2+}$  indicator

\* To whom correspondence should be addressed: [tnagai@es.hokudai.ac.jp](mailto:tnagai@es.hokudai.ac.jp)



## Abstract

**Background:** Efficient bioluminescence resonance energy transfer (BRET) from a bioluminescent protein to a fluorescent protein with high fluorescent quantum yield has been utilized to enhance luminescence intensity, allowing single-cell imaging in near real time without external light illumination.

**Methodology/Principal Findings:** We applied BRET to develop an autoluminescent  $\text{Ca}^{2+}$  indicator, BRAC, which is composed of  $\text{Ca}^{2+}$ -binding protein, calmodulin, and its target peptide, M13, sandwiched between a yellow fluorescent protein variant, Venus, and an enhanced *Renilla* luciferase, RLuc8. Adjusting the relative dipole orientation of the luminescent protein's chromophores improved the dynamic range of BRET signal change in BRAC up to 60%, which is the largest dynamic range among BRET-based indicators reported so far. Using BRAC, we demonstrated successful visualization of  $\text{Ca}^{2+}$  dynamics at the single-cell level with temporal resolution at 1 Hz. Moreover, BRAC signals were acquired by ratiometric imaging capable of canceling out  $\text{Ca}^{2+}$ -independent signal drifts due to change in cell shape, focus shift, etc.

**Conclusions/Significance:** The brightness and large dynamic range of BRAC should facilitate high-sensitive  $\text{Ca}^{2+}$  imaging not only in single live cells but also in small living subjects.

## Introduction

Bioluminescent proteins such as luciferase are a powerful tool for monitoring biological processes including gene expression in living organisms since bioluminescent signals can be acquired without an external light source; bioluminescence imaging is thus completely free from phototoxicity, photo-induced physiological reaction, and autofluorescence from the specimen, enabling signal detection from deep inside the tissue with high signal-to-noise ratio. These properties make bioluminescent proteins potentially superior to fluorescent proteins as a bioimaging tool. However, bioluminescence signals are too dim to be measured in real time, i.e., bioluminescence imaging generally requires longer exposure (more than several tens of seconds) than fluorescence imaging that takes less than 1 second. To overcome this drawback, an auto-illuminating fluorescent protein, eBAF-Y, has been developed [1]. eBAF-Y is based on the highly efficient bioluminescence resonance energy transfer (BRET) between enhanced *Renilla reniformis* luciferase (RLuc8) [2] and enhanced yellow fluorescent protein (EYFP). eBAF-Y emits a 3.5-fold brighter signal than RLuc8 alone, enabling observation of subcellular structure at the single-cell level in near real time at 0.1 Hz. This strategy has been applied to develop a similar auto-illuminating fluorescent protein, BRET3, composed of a mutant red fluorescent protein (mOrange) and RLuc8 [3]. BRET3 exhibits red-shifted light output peaking at 564 nm, making it easier to observe biological phenomena deep inside a small animal. Aequorin, another well-known bioluminescent protein, emits luminescence peaking at 466 nm in the presence of  $\text{Ca}^{2+}$  so it has been used as a  $\text{Ca}^{2+}$  indicator to monitor free  $\text{Ca}^{2+}$  concentration ( $[\text{Ca}^{2+}]$ ) in living specimens [4]. The highly efficient BRET has also been applied to aequorin by means of

fusion with green fluorescent protein (GFP), thereby increasing the luminescence intensity by about 50 fold [5]. Although aequorin-GFP is bright enough to allow real-time imaging, it is not suitable for long-term imaging since aequorin must be regenerated after emission upon  $\text{Ca}^{2+}$  binding, which takes more than several tens of minutes [6,7]. To circumvent this weak point, a  $\text{Ca}^{2+}$  indicator was developed based on split RLuc and Gluc [8,9]. Signal change of these indicators is based on complementation of the N- and C-terminal halves of the split luciferase via  $\text{Ca}^{2+}$ -induced interaction between CaM and M13. Although these indicators can detect  $\text{Ca}^{2+}$ -dependent signal changes in living cells, they could not calibrate  $[\text{Ca}^{2+}]$  because imaging of these indicators is based on single-emission measurement and thus the signal intensity change is highly dependent on the stoichiometric composition of the N- and C-terminal halves of the split luciferase in the cells. Also, these indicators cannot cancel out signal drift mainly caused by change in cell shape, focus drift, and uptake and consumption of coelenterazine-h due to auto or catalytic oxidization. To allow quantitative long-term real-time  $\text{Ca}^{2+}$  imaging, we designed a  $\text{Ca}^{2+}$  indicator based on BRET between RLuc8 and Venus, a brighter version of EYFP [10]. As the  $\text{Ca}^{2+}$ -sensing domain, we used a  $\text{Ca}^{2+}$  binding protein, calmodulin (CaM), and its target peptide, M13, as in the case of the well-known FRET-based  $\text{Ca}^{2+}$  indicator, cameleon [11]. Binding and release of  $\text{Ca}^{2+}$  from CaM induces reversible conformational change of the CaM-M13 fusion domain between an extended and compact form, which, in turn, changes the distance between Venus and RLuc8 whereby their emission is reciprocally changed due to BRET. Thus, this indicator enables ratiometric observation that can cancel out artifactual signal drift. To obtain a large BRET change, we tried several circularly permuted Venus variants

[12] to optimize the relative dipole orientation between the coelenterazine in RLuc8 and the chromophore of Venus. The best one, which we named BRAC, has a wild-type Venus and showed 60% signal change upon  $\text{Ca}^{2+}$  binding. Due to the brightness and large dynamic range, we successfully visualized  $\text{Ca}^{2+}$  oscillation induced by agonist stimulation of HeLa cells with improved time resolution and high signal-to-noise ratio.

## Results

### Construction of BRET-based reversible $\text{Ca}^{2+}$ indicators

To create a BRET-based autoluminescent reversible  $\text{Ca}^{2+}$  indicator, we chose the CaM-M13 chimeric protein for the  $\text{Ca}^{2+}$ -sensing domain as in the case of the FRET-based  $\text{Ca}^{2+}$  indicator, cameleon YC3.60 (see Ref. 12). ECFP in YC3.60 was first replaced with RLuc8, the brightest version of luciferase [2], to yield RLuc8-CaM-M13-cp173Venus (Figure 1). The construct was bacterially expressed and purified for measuring the signal change in the peak intensity ratio (530/480 nm) with  $\text{Ca}^{2+}$ . The dynamic range of the BRET signal change in RLuc8-CaM-M13-cp173Venus was 10% (Figure 2). Then, according to the strategy for expanding the dynamic range of FRET-based indicators [12], we replaced the Venus moiety in RLuc8-CaM-M13-Venus with a wild-type Venus or circularly permuted Venus variants that have a different translation start site from the original cp173Venus, as shown in Figure 1A. Among them, RLuc8-CaM-M13-Venus and RLuc8-CaM-M13-cp157Venus showed a 3-fold enhanced dynamic range (Figure 2). To further expand the dynamic range, we attempted to exchange the donor and acceptor in the above constructs to place the donor and acceptor molecule at the C- and N-terminus,